PCCP

PAPER

View Article Online
View Journal | View Issue

Cite this: *Phys. Chem. Chem. Phys.*, 2017, **19**, 13372

Low energy electron attenuation lengths in core–shell nanoparticles†

Michael I. Jacobs,[ab] Oleg Kostko,[b] Musahid Ahmed[b] and Kevin R. Wilson*[b]

Received 30th January 2017,
Accepted 5th May 2017

DOI: 10.1039/c7cp00663b

rsc.li/pccp

A velocity map imaging spectrometer is used to measure photoemission from free core–shell nanoparticles, where a salt core is coated with a liquid hydrocarbon shell (*i.e.* squalane). By varying the radial thickness of the hydrocarbon shell, electron attenuation lengths (EALs) are determined by measuring the decay in photoemission intensity from the salt core. In squalane, electrons with kinetic energy (KE) above 2 eV are found to have EALs of 3–5 nm, whereas electrons with smaller KE (<2 eV) have significantly larger EALs of >15 nm. These results (in the context of other energy-resolved EAL measurements) suggest that the energy dependent behavior of low energy electrons is similar in dielectrics when KE > 2 eV. At this energy the EALs do not appear to exhibit strong energy dependence. However, at very low KE (<2 eV), the EALs diverge and appear to be extremely material dependent.

Introduction

Electrons scatter both elastically and inelastically as they propagate through a material. The inelastic mean free path (IMFP) is the mean distance an electron with a specific kinetic energy (KE) travels between inelastic scattering events.[1] Understanding the energy dependence of the IMFP in materials is important in several different disciplines. For example, the short distance an electron travels between inelastic collisions makes photoelectron spectroscopy a surface sensitive technique.[2,3] If the energy dependence of the IMFP is known, then photoemission experiments can be used to obtain depth-resolved chemical information by varying the photoelectron KE.[4] Likewise, the IMFP of electrons is central to understanding photoemission heating of interstellar dust clouds that arises from the absorption of UV radiation. The magnitude of the electron IMFP is predicted to have a direct effect on the extent of warming.[5] Additionally, inelastic collisions of low energy electrons with DNA produce irreversible, detrimental effects due to bond scission reactions.[6–8] The extent of this damage is dependent on both the electron IMFP in the biological medium as well as the cross sections for the interactions.[9]

Most measurements of the IMFP have been made at high KE by depositing a thin film of material on a substrate and monitoring photoemission from the substrate as a function of film thickness, or by monitoring intensity of backscattered electrons.[10] Measurements of the IMFP of electrons with KE < 100 eV in soft materials (such as liquids) are difficult due to experimental challenges (such as high vapor pressures or difficulties collecting all photoelectrons using a hemispherical analyzer). Studies examining the propagation of low KE electrons in materials generally measure the electron attenuation length (EAL). The EAL is the film thickness that results in a 1/*e* decrease in signal intensity at a given energy compared to a non-coated substrate.[1] It is closely related to the IMFP, but because EAL convolutes elastic and inelastic scattering, it is calculated to be 15–30% shorter (depending on the KE of the electron and material).[1,11] The first low KE EALs measurements were made by impinging electrons onto a thin film and measuring the resulting transmission current.[12–20] These measurements generally resulted in a single "low energy" EAL that was highly material specific (for example, the low energy EALs for pentacene and perylene were reported to be 7.5 and 80 nm, respectively).[20] With the introduction of liquid jet experiments, measurements of the EAL in high vapor pressure liquids (such as water) became possible by either monitoring the angular dependence of photoemission[21,22] or coupling the O1s photoionization cross-section to the signal intensity from liquid water at different energies.[23] Additionally, recent work used the angular distribution of photoemission from free nanoparticles to model low energy electron IMFPs.[24,25] While still somewhat experiment specific, these energy-resolved measurements have yielded EALs that range from 1–5 nm for 1–25 eV KE photoelectrons in water.

Two complementary techniques are typically used to study the properties of low energy electrons in thin films: low energy electron transmission (LEET) and photoelectron transmission.[12] In LEET experiments, thin films are irradiated by electrons and either backscattered electrons or transmission current through the film are detected. In this technique, only the electrons that enter (and not those that exit) the thin film are fully-defined in terms of energy and momentum. Thus, information on an

[a] *Department of Chemistry, University of California, Berkeley, CA 94720, USA*
[b] *Chemical Sciences Division, Lawrence Berkeley National Laboratory, Berkeley, CA 94720, USA. E-mail: krwilson@lbl.gov; Tel: +1 510 495 2474*

† Electronic supplementary information (ESI) available. See DOI: 10.1039/c7cp00663b

electron's interactions within the film is lost because the measured value is generally a current that is independent of energy. Conversely, photoelectron transmission experiments input low energy electrons into a film *via* photoemission from a substrate (such as a platinum electrode). The low energy electrons that escape the film into vacuum are then detected.

Recent work has used aerosol photoemission to study surface chemistry,[26,27] surface segregation,[28,29] and electronic properties of nanoparticles.[24,25,30–32] Many of these studies use a velocity map imaging (VMI) spectrometer and vacuum ultraviolet light[24–26,30,31,33–35] or X-rays[26,32] from a synchrotron to measure the energy and angular distributions of photoelectrons from free nanoparticles. In this work, we use a VMI spectrometer to measure photoemission from free core–shell nanoparticles and measure the EAL in a liquid hydrocarbon, squalane. By coating squalane onto nanoparticles with a defined photoemission spectrum, we are able to measure the EAL for 1–5 eV photoelectrons. Our measurements, when combined with previous measurements of EAL in covalently-bonded, soft materials, show that the EALs of photoelectrons with >2 eV KE are roughly constant and independent of energy. However, for electrons with KE <2 eV, the behavior of photoelectrons is observed to be material dependent.

Experimental methods

Size-selected, core–shell nanoparticles of a specific composition are generated using a method that has been previously described.[36] The experimental setup is shown in Fig. 1. Briefly, an aqueous solution of the core material (either potassium iodide or sodium chloride) is first atomized and dried over silica gel to a relative humidity (RH) $<15\%$. This yields a stream of polydisperse, solid particles, which are then size-selected using a scanning mobility particle sizer (SMPS, TSI Inc.). The core diameters used in this experiment are 100, 150 and 200 nm. After size selection, part of the aerosol flow is sampled by a condensation particle counter (CPC) to monitor particle number concentrations. The remaining flow passes through a charcoal denuder to eliminate any unwanted volatile organic contaminants. The core aerosol is then passed through a tube furnace containing a pyrex tube with the coating material (*i.e.* liquid squalane). The coating forms on the core *via* heterogeneous nucleation upon exiting the heated section of the oven. The thickness of the coating is controlled by varying the temperature of the oven, and the size of the core–shell particle is measured using a second SMPS. The coating thickness is determined from the difference in diameter between aerosol that passes through the furnace and the uncoated aerosol stream that bypasses the oven. Radial coating widths vary from $\sim$1 to 9 nm with roughly $\pm$0.3 nm uncertainties (Fig. S4, ESI†). This treatment assumes that the nanoparticles are spherical, while in reality they most likely exist as rounded cubes. Previous work studying electron impact ionization of organic coated alkali halides using a similar coating technique found the monolayer coating thickness for a liquid hydrocarbon to be $\sim$0.7 nm.[37] Because most measurements reported here have coating thicknesses >0.7 nm, the aerosol particles are assumed to be completely coated. Some systematic errors in the coating thickness could exist due to the non-spherical nature of the particles and the potential for non-uniform coating.

Photoemission from free aerosol particles is measured using a VMI spectrometer (described previously).[26] Three electrodes in the spectrometer are tuned to achieve velocity mapping conditions,[38] where a projection of the nascent velocity distribution of photoelectrons is imaged on a multi-channel plate/phosphor detector with a CMOS camera. Photoelectron images of coated aerosol are collected for 150 s, and sample images at each coating thickness are collected in duplicate. The photoemission images are converted to photoelectron spectra using typical image processing techniques.[39] As shown in Fig. 2, the images are asymmetric due to the short absorption length of vacuum ultraviolet light. As has been discussed previously, this leads to preferential photoemission from the front of the nanoparticle and shadowing of the back of the particle.[25,31,33] A discussion of the effect that image asymmetry has on the extracted KE spectra is included in the ESI.† Images from the uncoated core are collected after each coating thickness, and the photoelectron spectra from the uncoated core are used to normalize the coated signal for any drifts in instrument or particle generation. Experiments were performed at the Chemical Dynamics Beamline (9.0.2) at the Advanced Light Source, Lawrence Berkeley National Lab.

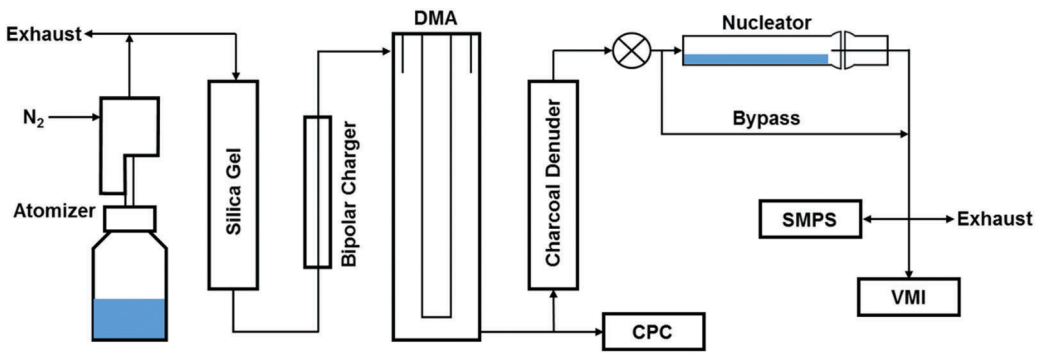

Fig. 1 Schematic of the coating experimental setup. (DMA = differential mobility analyzer, CPC = condensation particle counter, SMPS = scanning mobility particle sizer, VMI = velocity map imaging spectrometer.)

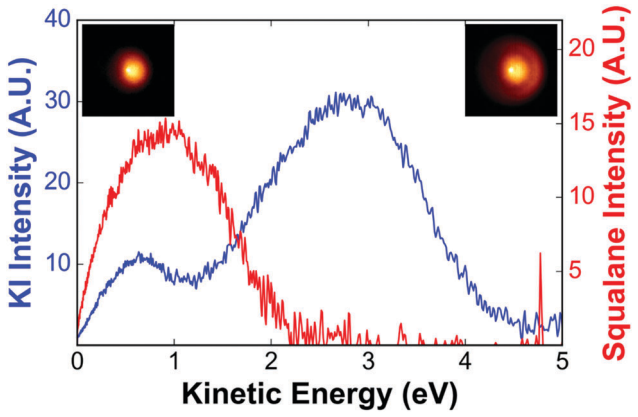

Fig. 2 Photoemission spectra of monodispersed KI and polydisperse squalane nanoparticles. The incident photon energy is 11 eV. The insets on the left and right show the images that correspond to the squalane and KI photoemission spectra, respectively. Despite similar intensities, the squalane nanoparticle spectrum is obtained using ~100× more material than the KI nanoparticle spectrum. Because squalane has a lower ionization cross-section and a higher threshold energy than KI, squalane photoemission does not interfere with the decay of KI photoemission intensity at the higher KEs.

To determine EALs in a coating, squalane is coated onto a KI core and photoemission from the particles is measured as a function of coating thickness. As the coating thickness increases, the intensity of photoemission from the core material decreases due to inelastic collisions. EALs of photoelectrons are determined by tracking the decay of photoemission from the core as a function of coating thickness. KI is chosen as the core material due to its low ionization threshold (6.8 eV)[40] compared to squalane (8.4 eV).[41] Fig. 2 shows the KE distribution of photoelectrons from pure, monodispersed KI nanoparticles (diameter, D_p = 150 nm, ~10^4 particles per cm^3) and pure, polydisperse squalane nanoparticles (D_p ~ 220 nm, ~10^6 particles per cm^3). The KE of photoelectrons from KI extends to higher energies than that of squalane due to the difference in threshold energies. The absolute photoemission intensity from squalane is very small compared to that of KI. Measurable photoemission intensities from pure squalane nanoparticles could only be recorded using a polydisperse aerosol distribution, which has ~100× more particles than the size selected KI flow (Fig. 2). Since the amount of squalane coating the KI core is only a small fraction of the squalane in the polydisperse flow, photoemission from squalane is not observable in the experiments to determine EAL. Even so, when determining EALs, we only measured KEs that are large enough to ensure there is no photoemission contribution from squalane. To cover a large range of KEs, photoemission from the core shell nanoparticles is measured at five different photon energies: 8.5, 9, 10, 11, and 12 eV. Photoemission at higher photon energies is not collected due to the interference with water vapor (IE = 12.6 eV).

Results and analysis

Fig. 3a–e shows photoemission from KI nanoparticles as a function of squalane coating thicknesses at incident photon energies of 8.5, 9, 10, 11, and 12 eV. The initial shape of the uncoated photoemission spectrum (black lines in Fig. 3) is determined by the photoionization cross-section of KI at these various energies. At the energies used in this study, the photoelectrons originate from the I 5p state.[40] As the coating thickness increases, two things are readily apparent from these spectra: (i) the intensity of the signal decreases with increasing coating thickness and (ii) there appears to be shift of the peak energy with increasing coating thickness. This first observation is due to the inelastic collisions of electrons inside the squalane shell. The latter observation can be attributed to the production of low KE electrons from inelastic collisions.[12] If electrons do not lose all of their KE when they inelastically collide, they can still escape from the particle. In this case, the intensities at lower energies would appear to decay slower because as the shell thickness increases, a portion of their intensities would come from higher KE electrons that have undergone inelastic collisions. To minimize the effects from the cascade to lower energy, a "top most interval" analysis is employed and only the highest energy electrons (those within ~0.5 eV of the largest KE in the initial spectra) are used to determine EALs. Fig. 4 shows the normalized photoemission intensity at 1.1 and 4.4 eV KE from the 8.5 and 12 eV spectra, respectively. If the EAL in squalane was independent of energy, these curves would have the same decay constant.

By definition, the EAL is the coating thickness that results in a $1/e$ decrease in signal compared to an uncoated substrate. Thus, the photoemission intensity from the core at a specific energy, $I(E, d)$, is measured as a function of coating thickness, d:

$$I(E,d) = I(E,0)e^{-\frac{y_e(d)}{L_e(E)}}, \quad (1)$$

where $I(E, 0)$ is the initial photoemission intensity at energy E without any coating, $y_e(d)$ is the distance the electron must travel through at a given coating thickness, and $L_e(E)$ is the EAL at energy E. As the coating thickness increases, an increasing amount of the incident light is absorbed by the coating. Thus, eqn (1) is modified to include the decrease in photon intensity that reaches the core due to the increased coating absorption:

$$I(E,d) = \left[I(E,0)e^{-\frac{y_\nu(d)}{L_\nu}}\right]e^{-\frac{y_e(d)}{L_e(E)}}. \quad (2)$$

In eqn (2), L_ν is the attenuation length of light in the coating and $y_\nu(d)$ is distance light travels through at a given coating thickness before encountering the core. At a given photon energy, L_ν is equal to $\lambda/4\pi\kappa$, where λ is the wavelength of the incident light and κ is the imaginary component of the refractive index of the coating material. Table S1 (ESI†) shows the energy-dependent κ values of squalane and the associated attenuation length of light, L_ν, at the energies we measured.[42] While uncertainties in κ values used in this study were not reported,[42] as will be discussed later, the calculated absorption lengths are generally larger than the measured EALs, which makes eqn (2) insensitive to changes in L_ν.

For the case of a flat surface, the escape length of electrons and penetration length of light is equal to the coating thickness (*i.e.* $y_\nu(d) = y_e(d) = d$). Surface curvature has previously been used

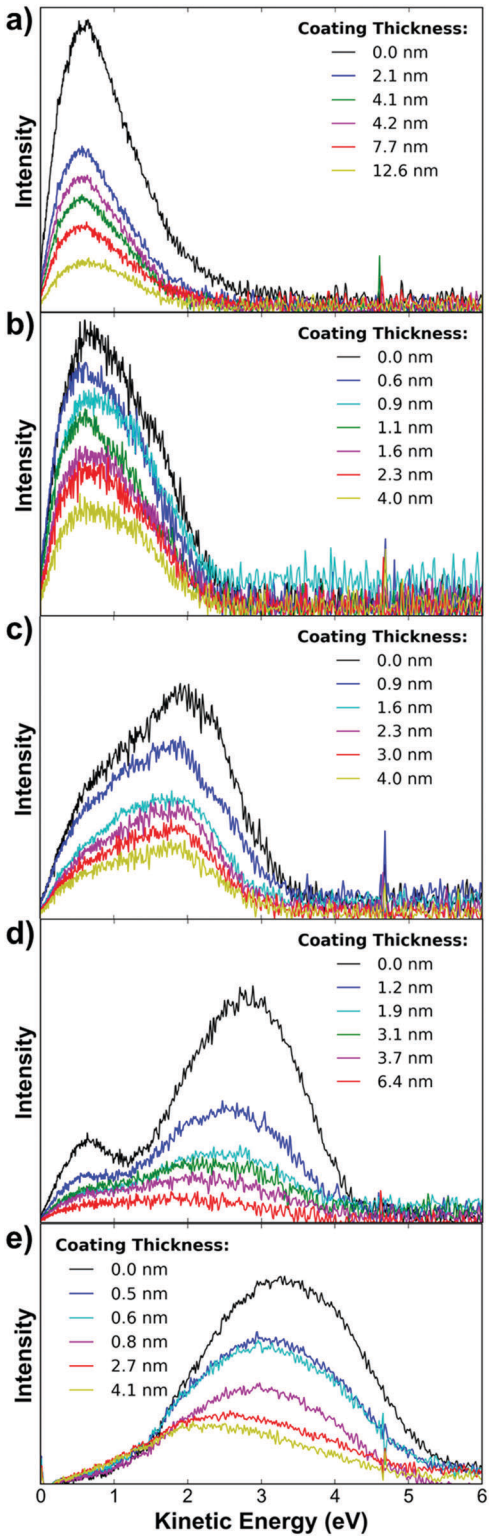

Fig. 3 Photoemission spectra of KI-squalane core–shell nanoparticles with varying squalane shell thicknesses. Spectra were collected at incident photon energies of 8.5 eV (a), 9 eV (b), 10 eV (c), 11 eV (d), and 12 eV (e). Note: the side band is missing in the 12 eV spectrum due to large gas phase background at low KE caused by higher harmonics from beamline 9.0.2.

to explain photoemission from nanoparticles[33] and electron impact charging of nanoparticles.[37] Because the thickness of

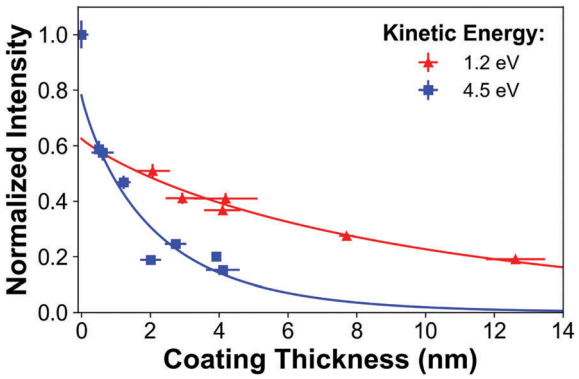

Fig. 4 Normalized intensity at 1.2 and 4.5 eV KE from the 8.5 and 12 eV photoemission spectra, respectively. EAL are extracted from the decay of KI photoemission intensity at different KEs using eqn (6). An energy dependence in the EAL in squalane results in differences in the decay rates at different KEs.

the shell is much smaller than the particle radius, surface curvature is negligible on the scale of electron scattering and coating thickness closely resembles the overlayer thickness in the EAL definition. Thus, the radial coating thickness (d) is used to describe distance electrons must escape at each shell thickness. However, as shown in Fig. 5, the distance the photon travels through the coating will only be equal to the coating thickness when the photon enters the core shell nanoparticle normal to its surface. From the geometries shown in Fig. 5, it can be shown that the distance a photon must travel through the coating to reach the core, $y(d, \theta)$, is:

$$y(d,\theta) = (R+d)\cos[\beta(\theta)] - \sqrt{R^2 - (R+d)^2\sin^2[\beta(\theta)]}, \quad (3)$$

where R is the radius of the core and $\beta(\theta)$ is the refracted angle between the incident light and the particle surface. The refracted

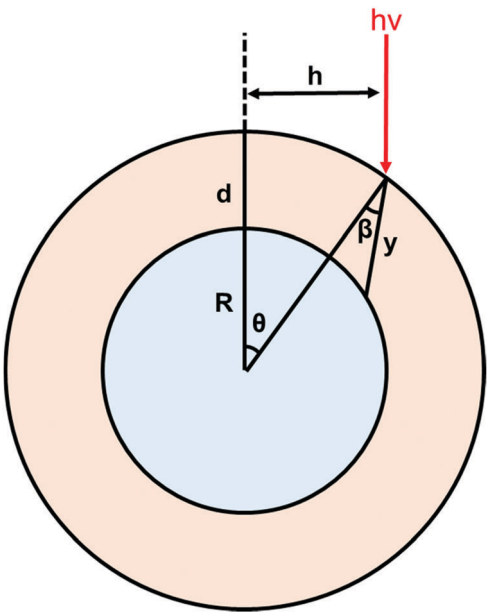

Fig. 5 Diagram showing the geometry of light entering the core through the squalane layer.

angle is determined using Snell's law with the previously measured refractive indices in squalane.[42] Previous work by Ziemann *et al.*[37] has shown that the probability, $g(\theta)\mathrm{d}\theta$, a photon enters the particle at an angle between θ and $\mathrm{d}\theta$ is:

$$g(\theta)\mathrm{d}\theta = 2\pi h\mathrm{d}h/\pi R^2 = 2\sin\theta\cos\theta\mathrm{d}\theta, \quad (4)$$

where h is defined in Fig. 5. The average attenuation of light as it travels through the coating, $\left\langle e^{-\frac{y_v(d)}{L_v}}\right\rangle$, before striking the core is given by:

$$\left\langle e^{-\frac{y_v(d)}{L_v}}\right\rangle = \int_0^{\pi/2} e^{\frac{y(d,\theta)}{L_v}} g(\theta)\mathrm{d}\theta. \quad (5)$$

This integral does not have an exact solution and is solved numerically at each coating thickness. EALs are determined by using eqn (5) to describe $\left\langle e^{-\frac{y_v(d)}{L_v}}\right\rangle$ and fitting the normalized intensity plots (*e.g.* Fig. 4) at each KE to the following:

$$\frac{I(E,d)}{I_0(E,0)} = \alpha\left\langle e^{-\frac{y_v(d)}{L_v}}\right\rangle e^{-\frac{d}{L_e(E)}}, \quad (6)$$

where α is a fitting parameter that is constrained to be less than one.[14] As the core particles are coated by a squalane shell, there is some probability that electrons can be scattered back into the core. Thus, the intensity from the uncoated aerosol is not used in the fit, and α accounts for the diminished number of electrons that enter the shell due to interfacial scattering (Fig. 4).

The EALs calculated from the five different photon energies are given in Table 1. This energy range provides measurements of electron attenuation from electrons with 1.1 to 4.4 eV KE. In general, at KE >2 eV, the EAL is determined to be 3–5 nm and does not appear to be a strong function of energy. At lower KE, the EAL increases, and at KE $<$ 2 eV, it is >15 nm.

Because the uncertainties in κ are not previously reported,[42] the sensitivity of eqn (6) to changes in the attenuation length of light was evaluated by applying a $\pm$20% error to κ and determining the resulting change in computed EALs. At a photon energy of 11 eV, the EAL of electrons with 3.4 $\pm$ 0.2 eV KE was calculated to be 3.8 $\pm$ 1.0 nm using κ = 0.7 and L_ν = 12.8 nm. If κ changes to 0.56 and 0.84 (a $-$20% and +20% error), the measured EAL at 3.4 eV changes to 3.5 and 4.0 nm, respectively. These differences are smaller than the uncertainty in the original measurement and show that the model does not have a strong sensitivity to changes in κ because the EAL is generally significantly shorter than L_ν.

Table 1 Experimental measurement of the energy dependence of the EAL in squalane. The errors represent uncertainties in the fit to eqn (6) ($\pm$1 s). Possible systematic errors are discussed in the text

Kinetic energy (eV)	EAL (nm)
1.1 $\pm$ 0.2	15.6 $\pm$ 3.1
2.1 $\pm$ 0.2	4.4 $\pm$ 2.1
2.9 $\pm$ 0.2	2.4 $\pm$ 0.4
3.4 $\pm$ 0.2	3.8 $\pm$ 1.0
4.4 $\pm$ 0.2	3.3 $\pm$ 0.4

Furthermore, because the dimensions of the particle are on the order of the wavelength of light, an accurate description of the intensity in the core would require full Mie scattering calculations. To provide a minimum for the reported EALs, we removed the absorption of light by the shell (*i.e.* constrained $\left\langle e^{-\frac{y_v(d)}{L_v}}\right\rangle = 1$ in eqn (6)), and assumed the attenuation of signal with increased coating thicknesses arose only from inelastic scattering of electrons. This treatment had the result of lowering the EALs by roughly 20–30% and represents a potential systematic error from the data analysis.

Finally, to confirm the measured EALs are specific to the squalane coating and are not dependent on the experimental approach, the size and material of the core were varied. Table S2 (ESI†) shows the EALs in squalane measured with different sized KI cores (100 nm, 150 nm and 200 nm). Additionally, Table S2 (ESI†) shows the EALs in squalane using both a KI and NaCl core. While the NaCl photoemission spectra are slightly complicated by squalane photoemission (the ionization thresholds of KI, NaCl and squalane are 6.8, 8.2 and 8.4 eV, respectively),[40,41] the general agreement in escape lengths suggests the observed EALs are specific to the properties of the squalane shell.

Discussion

The EALs in squalane measured in this study range from 3.3 nm at 4.4 eV to 15.6 nm at 1.1 eV. As shown in Table 1, the EALs are roughly constant ($\sim$3–5 nm) when KE $>$ 2 eV. However, when KE $<$ 2 eV, the attenuation lengths increase to >15 nm. Low energy EALs in solid organic films have previously been measured by monitoring electron transmission currents through films of different thicknesses.[13–17,19,43] Energy-resolved EALs in *n*-$C_{36}H_{74}$ were collected by scanning the incident photon energy on a Pt substrate and changing the film thickness (data shown in Fig. 6).[16,17] The measured attenuation lengths of 2–5 eV electrons in *n*-$C_{36}H_{74}$ are $\sim$3–5 nm, which are in good agreement with the attenuation lengths reported here for squalane (also 3–5 nm for a similar energy range). However, when the KE is $<$2 eV, the EALs in *n*-$C_{36}H_{74}$ remain constant ($\sim$2.5 nm),[16] which differs from the measurements for squalane reported here. At low photoelectron energies, Pfluger *et al.* describe phonon excitation associated with the C–H stretching mode as the primary energy-loss scattering source.[19] However, Cartier *et al.* mention that at lower KE, the measured EALs varied with experimental conditions and the length of time a sample was irradiated due to a changing number of trap states.[16] Because the VMI spectrometer constantly probes a new surface, we don't expect a similar ''history'' effect in our experiments. The first studies looking at transmission of low energy electrons through organic films were not energy-resolved, and thus only an average ''low energy'' ($<$3 eV) EAL was measured. The reported attenuation lengths (generally 10–100s of Å) are extremely dependent on film composition.[13–15,20,43] For example, low energy electrons ($<$3 eV) had EALs of 7.5 and 80 nm in films

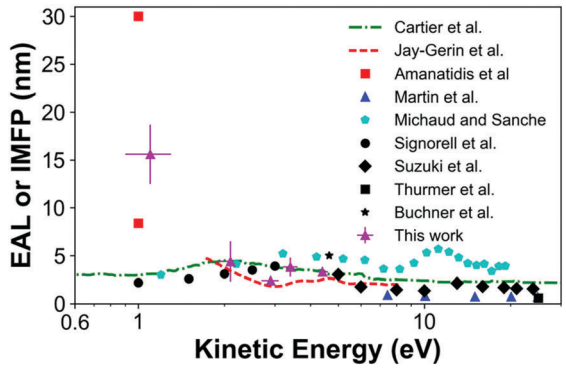

Fig. 6 Collection of energy-resolved, low energy EAL in soft materials. The measurements from this work are given by the magenta triangles. Error bars represent ±1 s. The green and red dashed lines represent EALs in paraffin, n-$C_{36}H_{74}$ (Cartier *et al.*[16,17]) and IMFPs in methane (Jay-Gerin *et al.*[45]) films, respectively. The red squares represent the EAL in thick (top) and thin (bottom) squalane layers (Amanatidis *et al.*[46]). The blue triangles represent EALs measured in a free standing carbon film (Martin *et al.*[48]). The black symbols represent EALs in liquid water from aerosol particles (circles, Signorell *et al.*[25]) and liquid jets (diamonds, Suzuki *et al.*;[23] square, Thurmer *et al.*;[22] star, Buchner *et al.*[47]). The pentagons represent EALs in solid water (Michaud and Sanche[49]). At energies >2 eV, the EAL all remain fairly constant.

composed of pentacene and perylene, respectively.[20] Additionally, experiments looking at low energy electron transmission in methane[44] and krypton[45] films show IMFPs (and thus EALs) that increase at electron KE < 2 eV (from 2 nm at 3 eV to 5 nm at 1.7 eV). These studies suggest that at lower KE, there is a corresponding lower density of states and thus fewer possible modes to deposit energy in a given scattering event. Thus, based on the large variability of previously reported EALs, the low KE (<3 eV) EAL appear to be extremely sensitive to the electronic structure of the material.

A very recent study also examined the photoemission from core–shell nanoparticles and estimated the EAL of photoelectrons with 0.5–1.0 eV KE using a total electron yield (TEY) measurement. For thin and thick shells of squalane, they report EALs of 8.0 ± 0.5 and 30 ± 3 nm, respectively.[46] The EAL reported here for a similar energy range (15.6 nm for 1.1 ± 0.2 eV electrons) falls between the two values reported by Amanatidis *et al.*[46] For a direct comparison with these previous results, TEY of the core is measured as a function of coating thickness at each photon energy. Because TEY combines the photoemission intensity of many different KEs, EALs cannot be directly extracted from this measurement. Instead, the decrease in TEY signal is fit to eqn (6) to determine an average attenuation coefficient. The average attenuation coefficients are presented in the ESI† (Table S3). The work of Amanatidis *et al.* uses a two photon (266 nm) ionization scheme, which results in ~9.3 eV radiation. The core material (sodium benzoate) used by Amanatidis *et al.* has a different ionization threshold (~7.5 eV)[46] than the KI core here (6.8 eV).[40] Thus, the TEY measurements at the specific photon energies are not directly comparable because the KE of the photoelectrons differ. However, the TEY measurements at 8.5 and 9 eV (which result in a KE spectra closest to that of Amanatidis *et al.*) yield average electron attenuation coefficients of 18.8 ± 5.1 nm and 4.9 ± 1.8 nm, respectively. These average attenuation coefficients bound the thin shell EAL reported by Amanatidis *et al.* and suggest the TEY measurements are very sensitive to the incident photon energy.

As a further means of comparison, there is an increasing body of evidence suggesting the EAL in liquid water approaches a constant value at low KEs.[21–23,47] The lowest energy EAL reported by Suzuki *et al.*[23] (3.02 ± 0.46 nm at 5 eV) as well as that reported by Buchner *et al.*[47] (5 nm at 4.65 eV) are in reasonable agreement with the measurements reported here. Additionally, recent work by Signorell *et al.* using angle resolved photoelectron spectroscopy of aqueous nanoparticles extracted the IMFP and EAL of low kinetic energy photoelectrons.[25] The EAL of electrons with 3 eV KE in water is reported to be 3.9 nm, which is in good agreement with the results reported here. However, at lower KEs (<3 eV), Signorell *et al.* reports a decrease in the EAL, which is attributed to an increase in purely vibrational scattering.[25]

Shown in Fig. 6 is a comparison of previously published energy-resolved EAL (and IMFP) measurements for covalently bonded, soft materials and water. Shown in this Figure are EALs (up to 25 eV) for carbon containing species,[16,44,46,48] liquid water[22,23,25,47] and solid water.[49] As noted above, there is significant scatter in measurements of the EAL at very low KE (<2 eV) where the EALs are expected to be much more material specific. However, a common feature for all measurements is the consistency of EALs for electrons with >2 eV KE. Based on the results shown in Fig. 6, it appears that (to some extent) low KE electrons in covalently bonded, soft materials have equally short EALs and are as surface sensitive as electrons with larger KE. These results have consequences for future photoemission experiments that utilize electron KE to obtain depth profiles. For example, these data suggest that depth profiling photoemission experiments most likely cannot be performed by moving the KE of photoelectrons to lower energy without explicitly measuring the energy dependence of very low KE photoelectrons.

Conclusion

In this paper, we have used a VMI spectrometer to probe photoemission from free core–shell nanoparticles. The VMI spectrometer detects all electrons that are emitted from the nanoparticles. By changing the thickness of the shell we have determined the low energy EAL in squalane. At very low kinetic energy (<2 eV), the EAL in squalane is >15 nm. At slightly larger kinetic energies (>2 eV), the EAL drops to 3–5 nm. Together with other energy resolved EALs in covalently bonded materials, these results suggest that the attenuation lengths of electrons with >2 eV KE do not change with increasing kinetic energy. This finding suggests that these low energy electrons are equally surface sensitive as higher KE photoelectrons. The energy dependence of EALs for electrons with KE <2 eV appear to be highly material specific.

The use of core–shell aerosol particles to determine EALs is limited when performed using VUV radiation (due to the absorption

of light by the shell material). However, this technique appears to have more promise and applicability at higher energies (such as soft X-rays) where the light penetration lengths are larger (*i.e.* light absorption by the shell can be neglected) and the spectral features (core–shell excitation) are more defined.

Acknowledgements

This work and the Advanced Light Source were supported by the Director, Office of Energy Research, Office of Basic Energy Science of the U.S. Department of Energy under Contract No. DE-AC02-05CH11231. M. I. J. thanks the NSF for an NSF Graduate Research Fellowship under DGE-1106400. K. R. W. was supported by the Department of Energy, Office of Science Early Career Research Program.

References

1 A. Jablonski and C. J. Powell, *J. Electron Spectrosc. Relat. Phenom.*, 1999, **100**, 137–160.
2 M. P. Seah and W. A. Dench, *Surf. Interface Anal.*, 1979, **1**, 2–11.
3 S. Tanuma, C. J. Powell and D. R. Penn, *Surf. Interface Anal.*, 1994, **21**, 165–176.
4 S. Ghosal, J. C. Hemminger, H. Bluhm, B. S. Mun, E. L. D. Hebenstreir, G. Ketteler, D. F. Ogletree, F. G. Requejo and M. Salmeron, *Science*, 2005, **307**, 563–566.
5 J. C. Weingartner and B. T. Draine, *Astrophys. J., Suppl. Ser.*, 2001, **134**, 263–281.
6 F. Martin, P. D. Burrow, Z. Cai, P. Cloutier, D. Hunting and L. Sanche, *Phys. Rev. Lett.*, 2004, **93**, 6–9.
7 L. G. Caron and L. Sanche, *Phys. Rev. Lett.*, 2003, **91**, 113201.
8 B. Boudaiffa, P. Cloutier, D. Hunting, M. A. Huels and L. Sanche, *Science*, 2000, **287**, 1658–1660.
9 E. Alizadeh, T. M. Orlando and L. Sanche, *Annu. Rev. Phys. Chem.*, 2015, **66**, 379–398.
10 C. J. Powell and A. Jablonski, *J. Phys. Chem. Ref. Data*, 1999, **28**, 19.
11 C. J. Powell, *J. Electron Spectrosc. Relat. Phenom.*, 1988, **47**, 197–214.
12 R. Naaman and L. Sanche, *Chem. Rev.*, 2007, **107**, 1553–1579.
13 W. B. Berry, *J. Electrochem. Soc.*, 1971, **118**, 597–600.
14 Y. C. Chang and W. B. Berry, *J. Chem. Phys.*, 1974, **61**, 2727.
15 J.-T. J. Huang and J. L. Magee, *J. Chem. Phys.*, 1974, **61**, 2736.
16 E. Cartier, P. Pfluger, J. J. Pireaux and M. Rei Vilar, *Appl. Phys. A: Solids Surf.*, 1987, **44**, 43–53.
17 E. Cartier and P. Pfluger, *Phys. Rev. B: Condens. Matter Mater. Phys.*, 1986, **34**, 8822–8827.
18 M. Rei Vilar, M. Schott and P. Pfluger, *J. Chem. Phys.*, 1990, **92**, 5722–5730.
19 P. Pfluger, H. R. Zeller and J. Bernasconi, *Phys. Rev. Lett.*, 1984, **53**, 94–97.
20 S. Hino, N. Sato and H. Inokuchi, *Chem. Phys. Lett.*, 1976, **37**, 494–498.
21 N. Ottosson, M. Faubel, S. E. Bradforth, P. Jungwirth and B. Winter, *J. Electron Spectrosc. Relat. Phenom.*, 2010, **177**, 60–70.
22 S. Thürmer, R. Seidel, M. Faubel, W. Eberhardt, J. C. Hemminger, S. E. Bradforth and B. Winter, *Phys. Rev. Lett.*, 2013, **111**, 1–5.
23 Y. I. Suzuki, K. Nishizawa, N. Kurahashi and T. Suzuki, *Phys. Rev. E: Stat., Nonlinear, Soft Matter Phys.*, 2014, **90**, 1–5.
24 M. Goldmann, J. Miguel-Sánchez, A. H. C. West, B. L. Yoder and R. Signorell, *J. Chem. Phys.*, 2015, **142**, 224304.
25 R. Signorell, M. Goldmann, B. L. Yoder, A. Bodi, E. Chasovskikh, L. Lang and D. Luckhaus, *Chem. Phys. Lett.*, 2016, **658**, 1–6.
26 M. I. Jacobs, B. Xu, O. Kostko, N. Heine, M. Ahmed and K. R. Wilson, *J. Phys. Chem. A*, 2016, **120**, 8645–8656.
27 F.-X. Ouf, P. Parent, C. Laffon, I. Marhaba, D. Ferry, B. Marcillaud, E. Antonsson, S. Benkoula, X.-J. Liu, C. Nicolas, E. Robert, M. Patanen, F.-A. Barreda, O. Sublemontier, A. Coppalle, J. Yon, F. Miserque, T. Mostefaoui, T. Z. Regier, J.-B. A. Mitchell and C. Miron, *Sci. Rep.*, 2016, **6**, 36495.
28 E. Antonsson, M. Patanen, C. Nicolas, J. J. Neville, S. Benkoula, A. Goel and C. Miron, *Phys. Rev. X*, 2015, **5**, 11025.
29 P.-C. Lin, Z.-H. Wu, M.-S. Chen, Y.-L. Li, W.-R. Chen, T.-P. Huang, Y. Lee and C. C. Wang, *J. Phys. Chem. B*, 2017, **121**, 1054–1067.
30 K. R. Wilson, D. S. Peterka, M. Jimenez-Cruz, S. R. Leone and M. Ahmed, *Phys. Chem. Chem. Phys.*, 2006, **8**, 1884–1890.
31 K. R. Wilson, S. Zou, J. Shu, E. Rühl, S. R. Leone, G. C. Schatz and M. Ahmed, *Nano Lett.*, 2007, **7**, 2014–2019.
32 B. Xu, M. I. Jacobs, O. Kostko and M. Ahmed, *ChemPhysChem*, 2017, DOI: 10.1002/cphc.201700197.
33 M. J. Berg, K. R. Wilson, C. M. Sorensen, A. Chakrabarti and M. Ahmed, *J. Quant. Spectrosc. Radiat. Transfer*, 2012, **113**, 259–265.
34 A. H. C. West, B. L. Yoder and R. Signorell, *J. Phys. Chem. A*, 2013, **117**, 13326–13335.
35 K. R. Wilson, H. Bluhm and M. Ahmed, in *Fundamentals and Applications in Aerosol Spectroscopy*, ed. R. Signorell and J. P. Reid, CRC Press, 2011, pp. 367–400.
36 L. Lee and K. Wilson, *J. Phys. Chem. A*, 2016, **120**, 6800–6812.
37 P. J. Ziemann, P. Liu, D. B. Kittelson and P. H. McMurry, *J. Phys. Chem.*, 1995, **99**, 5126–5138.
38 A. T. J. B. Eppink and D. H. Parker, *Rev. Sci. Instrum.*, 1997, **68**, 3477–3484.
39 V. Dribinski, A. Ossadtchi, V. A. Mandelshtam and H. Reisler, *Rev. Sci. Instrum.*, 2002, **73**, 2634.
40 R. Poole, J. Jenkin, J. Liesegang and R. Leckey, *Phys. Rev. B: Condens. Matter Mater. Phys.*, 1975, **11**, 5179–5189.
41 H. Koizumi, *Chem. Phys. Lett.*, 1994, **219**, 137–142.
42 L. R. Painter, J. S. Attrey, H. H. Hubbell and R. D. Birkhoff, *J. Appl. Phys.*, 1984, **55**, 756.
43 S. Hino, *J. Chem. Phys.*, 1977, **67**, 4139.
44 J.-P. Jay-Gerin, B. Plenkiewicz, P. Plenkiewicz, G. Perluzzo and L. Sanche, *Solid State Commun.*, 1985, **55**, 1115–1118.
45 E. Keszei, R. Marsolais, M. Deschenes, T. Goulet, L. Sanche and J.-P. Jay-Gerin, *J. Electron Spectrosc. Relat. Phenom.*, 1985, **36**, 269–279.
46 S. Amanatidis, B. L. Yoder and R. Signorell, 2017, arXiv: 1702.07865 [cond-mat.soft].
47 F. Buchner, T. Schultz and A. Lübcke, *Phys. Chem. Chem. Phys.*, 2012, **14**, 5837–5842.
48 C. Martin, E. T. Arakawa, T. A. Callcott and R. J. Warmick, *J. Electron Spectrosc. Relat. Phenom.*, 1986, **42**, 171–175.
49 M. Michaud and L. Sanche, *Phys. Rev. A: At., Mol., Opt. Phys.*, 1987, **36**, 4672–4683.

